Hyperpolarized ^{3}He Magnetic Resonance Functional Imaging Semiautomated Segmentation

Miranda Kirby, BSc, Mohammadreza Heydarian, PhD, Sarah Svenningsen, BMSc, Andrew Wheatley, BSc, David G. McCormack, MD, Roya Etemad-Rezai, MD, Grace Parraga, PhD

Rationale and Objectives: To improve intra- and interobserver variability and enable the use of functional magnetic resonance imaging (MRI) for multicenter, multiobserver studies, we generated a semiautomated segmentation method for hyperpolarized helium-3 (^{3}He) MRI. Therefore the objective of this study was to compare the reproducibility and spatial agreement of manual and semiautomated segmentation of ^{3}He MRI ventilation defect volume (VDV) and ventilation volume (VV) in subjects with asthma, chronic obstructive pulmonary disease (COPD), and cystic fibrosis (CF).

Materials and Methods: The multistep semiautomated segmentation method we developed employed hierarchical K-means clustering to classify ^{3}He MRI pixel intensity values into five user-determined clusters ranging from signal void to hyperintense. A seeded region-growing algorithm was also used to segment the ^{1}H MRI thoracic cavity for coregistration to the ^{3}He cluster-map, generating VDV and VV.

Results: We compared manual segmentation performed by an expert observer and semiautomated measurements of ^{3}He MRI VDV and observed strong significant correlations between the volumes generated using each method (asthma, $n = 5$, $r = 0.89$, $P < .0001$; COPD, $n = 5$, $r = 0.84$, $P < .0001$; CF, $n = 5$, $r = 0.89$, $P < .0001$). Semiautomated VDV had high interobserver reproducibility (coefficient of variation [CV] = 7%, intraclass correlation coefficient [ICC] = 0.96); intraobserver reproducibility was significantly higher for semiautomated (CV = 5%, ICC = 1.00) compared to manual VDV (CV = 12%, ICC = 0.98). Spatial agreement for VV determined using the Dice coefficient (D) was also high for all disease states (asthma, D = 0.95; COPD, D = 0.88; CF, D = 0.90).

Conclusions: Semiautomated segmentation ^{3}He MRI provides excellent inter- and intraobserver precision with high spatial and quantitative agreement with manual measurements enabling its use in longitudinal studies.

Key Words: hyperpolarized ^{3}He MRI; segmentation; ventilation defects; COPD; asthma; cystic fibrosis.

Pulmonary hyperpolarized helium-3 (^{3}He) magnetic resonance imaging (MRI) is a functional imaging method that detects ventilation abnormalities in elderly never smokers (1) and patients with chronic obstructive pulmonary disease (COPD) (2–9), asthma (10–13), cystic fibrosis (CF) (14–16), radiation-induced lung injury (17,18), and lung transplant recipients (19,20). Over the past few years, this approach has been enhanced by improvements in laser optical pumping techniques (21), parallel imaging (22), single-scan acquisition of ventilation and diffusion-weighted images (23), single-scan acquisition of ventilation and ^{1}H MRI anatomical images (24), and dynamic imaging (25,26). Although this large body of work has advanced the scope and type of functional images that can be acquired, there have been fewer improvements related to image analysis methods (27–29). As we move forward with functional noble gas imaging and transition to hyperpolarized xenon-129 (^{129}Xe) MRI, a less expensive and more readily available approach, image analysis methods are urgently required for quantitative evaluation across a wide variety of respiratory diseases.

Previous ^{3}He functional/ventilation analyses were based on a radiologist's interpretation of the ventilated lung regions (27,30), and quantification of ventilation defects was performed using scoring (1,8,11) and volumetric analysis approaches (1,8). While in these studies, imaging measurements were correlated with well-established measures of disease, a limitation of manual methods is the inherent reliance on highly trained observers that increases segmentation time and introduces the potential for inter- and intraobserver variability. Although straightforward automated threshold methods have been used for segmentation of ventilation (27), automated segmentation of the ^{3}He ventilation defects themselves, previously demonstrated by Tustison et al (28) as

Acad Radiol 2012; 19:141–152

From the Imaging Research Laboratories, Robarts Research Institute, 100 Perth Drive, London, Canada N6A 5K8 (M.K., M.H., S.S., A.W., G.P.); Department of Medical Biophysics (M.K., S.S., G.P.), Division of Respirology (D.G.M.), Department of Medicine, Department of Medical Imaging (R.E.-R., G.P.), and Graduate Program in Biomedical Engineering (G.P.), The University of Western Ontario, London, Canada. Received June 8, 2011; accepted October 5, 2011. Support received from the Natural Sciences and Engineering Research Council (NSERC) of Canada, Canadian Institutes of Health Operating Grant MOP #97748, Team Grant FRN #97687, and New Investigator Award. **Address correspondence to:** G.P. e-mail: gep@imaging.robarts.ca

doi:10.1016/j.acra.2011.10.007

a feature that differentiated asthma and healthy subject images, has proven to be much more difficult. Subjects with severe obstructive disease, such as COPD or asthma, have numerous ventilation defects that appear in ^{3}He images as signal voids. Hyperinflation is also commonly observed in obstructive lung disease in part from gas trapping and therefore changes in the thoracic cavity shape vary from patient to patient and within individual patients over time. Thus, segmentation of ventilation defects likely requires an understanding of the relationship between ^{3}He functional information with the anatomy of the thoracic cavity derived from proton (^{1}H) MRI. Furthermore, because there appear to be regions with ^{3}He signal voids, as well as regions of hypo- and hyperintensity, segmentation methods are required for the visually different classes of ^{3}He MRI signal.

Therefore, our objective was to develop a semiautomated segmentation method by applying two well-established image segmentation approaches, seeded region-growing (31) for segmentation of the thoracic cavity from ^{1}H MRI and K-means clustering (32) to classify ^{3}He MRI pixel intensities as previously investigated (33,34) to generate ^{3}He MRI ventilation measurements. The combination of these well-established and widely used segmentation methods allows for quantification and characterization of the important ventilation information contained in the image. ^{3}He MRI segmentation methods must have high intra- and inter-observer reproducibility across a variety of respiratory diseases and subjects. Therefore, here we evaluated the reproducibility as well as the spatial and quantitative relationships between manual and semiautomated functional measurements in subjects with asthma, COPD, and CF.

MATERIALS AND METHODS

Subjects

All subjects provided written informed consent to protocols approved by Health Canada and a local research ethics board. COPD subjects were ex-smokers, with a clinical diagnosis of COPD and categorized according to the Global initiative for chronic Obstructive Lung Disease (GOLD) criteria (35), with a smoking history of at least 10 pack-years as previously described (5). Adult asthmatics between 18–50 years of age were enrolled with forced expiratory volume in 1 second (FEV_1) $\%_{pred}$ >60% with a physician diagnosis of asthma and adult CF subjects (18–40 years of age) were also enrolled with $FEV_1\%_{pred}$ >50%.

Image Acquisition

MRI was performed on a whole-body 3.0 Tesla Excite 12.0 MRI system (GEHC, Milwaukee, WI) with broadband imaging capability as previously described (1), and ^{3}He MRI was enabled using a single-channel, rigid elliptical transmit/receive chest coil (RAPID Biomedical GmbH, Wuerzburg Germany). Pulse oximetry was used to measure arterial oxygen saturation for all subjects during scanning sessions and considered an adverse event occurred when arterial oxygen saturation decreased below 88% continuously for ≥15 seconds at any time during the scanning session. Study withdrawal was required when arterial oxygen saturation decreased to 80% for 10 seconds or longer. It is important to note that we endeavored to minimize the potential for differences in the levels of inspiration between the breath-hold scans for each subject by: 1) training and practice for all subjects before MRI related to the inspiration breath-hold maneuver from functional residual capacity, and, 2) continuous coaching and monitoring at the MRI scan bedside by a pulmonary function technologist during all inspiration breath-hold scans.

Conventional ^{1}H MRI was performed before hyperpolarized ^{3}He MRI with subjects scanned during 1.0 L breath-hold of $^{4}He/N_2$ using the whole-body radiofrequency coil and ^{1}H fast spoiled gradient recalled echo sequence (16 seconds of total data acquisition, repetition time [TR]/echo time [TE]/flip angle = 4.7 ms/1.2 ms/30°, field-of-view [FOV] = 40 × 40 cm, matrix 256 × 128, 14 slices, 15-mm slice thickness, 0 gap), as previously described (1).

Before ^{3}He MRI, a polarizer system (HeliSpin™, GEHC, Durham, NC) was used to polarize ^{3}He gas to 30%–40% and doses (5 mL/kg body weight) were administered in 1.0 L Tedlar® bags diluted with ultrahigh purity, medical grade nitrogen (Spectra Gases, Alpha, NJ). As previously described (1), hyperpolarized ^{3}He MRI coronal static ventilation images were acquired during breath-hold of a 1 L $^{3}He/N_2$ mixture (14 seconds' data acquisition, TR/TE/flip angle = 4.3 ms/1.4 ms/7°, bandwidth = 31.25, FOV = 40 × 40 cm, matrix 128 × 128, 14 slices, 15-mm slice thickness, 0 gap).

Manual Segmentation

Manual segmentation was repeated five times to estimate observer reliability using the approximation method developed by Walter et al (36). All subjects were first randomized and subsequently manually segmented by a single observer blinded to subject identity and disease status, and all subjects measurements were repeated five times each (15 subjects × 5 repetitions = 75 image datasets). To minimize memory bias, at least 24 hours was required between repetition rounds and randomization of subject image datasets was performed between each repetition round. The observer (M.K.) had 3 years' experience performing manual ^{3}He MRI segmentation having been trained by an experience chest radiologist (R.E.R.). As previously described (1), ventilation volume (VV) (30) was recorded after manual segmentation of the ventilated lung regions and ventilation defect volume (VDV) (1,8) was recorded after manual segmentation of the ^{3}He MRI focal ventilation defects, using custom-designed image visualization software (37), providing a method for two-dimensional rigid single-point image registration (^{1}H and ^{3}He slices) based on fiducial markers located on the carina. As previously described (38), a ventilation defect was

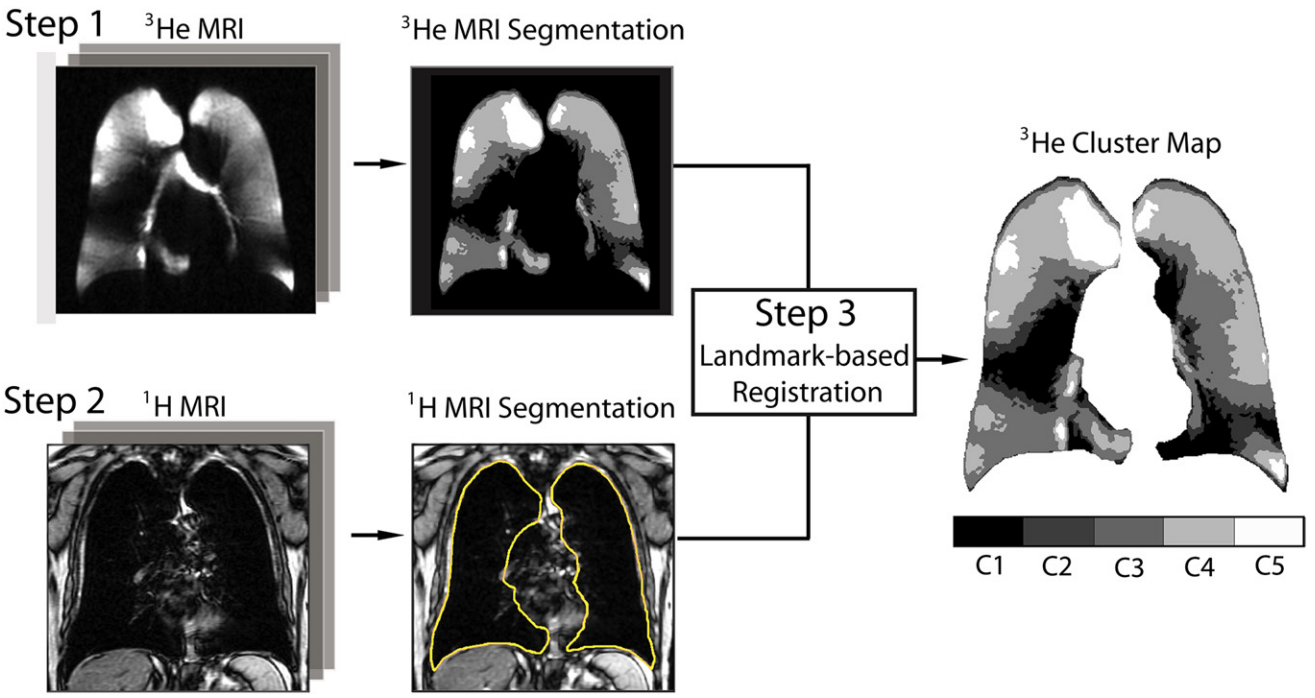

Figure 1. Schematic of hyperpolarized helium-3 (^{3}He) semiautomated segmentation methodology. Semiautomated segmentation was accomplished in three steps: 1) hierarchical K-means clustering of ^{3}He magnetic resonance imaging (MRI) into five clusters where cluster 1 (C1) represented regions of ventilation defect and background, and clusters 2 to 5 (C2-C5) represented gradations of signal intensity/ventilation; 2) ^{1}H MRI segmentation using seeded region-growing algorithm; and 3) landmark-based registration of ^{1}H and ^{3}He MRI segmentation to differentiate the ventilation defects from the background, and therefore generating a ^{3}He voxel cluster map.

identified by the observer as any lung region of diminished signal intensity but not including those areas of signal loss associated with the pulmonary vascular structures, heart, hilum, and mediastinum.

Semiautomated Segmentation: Overview of Method

Multistep segmentation software was generated using MATLAB R2007b (The Mathworks Inc., Natick, MA). All subjects, after randomization, were segmented using the semiautomated method by two observers blinded to subject identity and disease status, and measurements were repeated five times each (15 subjects × 5 repetitions × 2 observers = 150 image datasets). To minimize memory bias, at least 24 hours was required between repetition rounds. The observer (M.K.) had 1 year of experience developing and performing semiautomated ^{3}He MRI segmentation, and the observer (S.S.) had 1 month experience performing semiautomated ^{3}He MRI segmentation. Figure 1 provides a summary of our method. Briefly, ^{3}He MR images (step 1) were segmented automatically using a hierarchical version of K-means clustering algorithm (32), and ^{1}H MR images were segmented automatically using a seeded region-growing algorithm (SRGA) (31) (step 2). ^{1}H MR segmented images were registered (39) to ^{3}He MR segmented images (step 3) to differentiate the ventilation defects from the background and therefore generating a ^{3}He voxel cluster map, with clusters ranging from 1 to 5, representing gradations of signal intensity from no signal (cluster 1, C1) and hypointense signal (C2) to hyperintense signal (C5). This approach was first tested in a training dataset of five COPD subjects (5 subjects × 10 slices = 50 image slices) for comparison to manual segmentation. Results from the training dataset indicated that the semiautomated algorithm completed all tasks with image signal-to-noise-ratio ≥13, and this was the case for nearly all but the most anterior slices for each subject. The combination of four initial clusters and reclustering the initial C1 yielding a total of five clusters provided the best qualitative correlation with manual expert observer (chest radiologist) results. We also quantitatively compared K-means with the initial user input of 4 to 10 clusters and the hierarchical K-means approach (4 initial clusters and reclustering the initial C1) with manual segmentation on the training dataset, and determined that hierarchical K-means provided the highest correlation and lowest Bland-Altman bias with manual segmentation and was subsequently used for the testing dataset (Appendix Table).

^{3}He MRI Automated Segmentation: K-means Clustering Algorithm

^{3}He MRI of obstructive (COPD and asthma) and restrictive (CF) lung disease are typically characterized by heterogeneous ^{3}He MRI signal intensity that reflect gas distribution heterogeneity during the inspiration breath-hold scan. The expert observer typically can distinguish between four visually apparent classes of ^{3}He MRI signal–signal void, hypointense (or partial volume), normal intensity, and hyperintense signal.

TABLE 1. Subject Demographics

Parameter	All (n = 15) (±SD) (range)	Asthma (n = 5) (±SD) (range)	COPD (n = 5) (±SD) (range)	CF (n = 5) (±SD) (range)
Age, y	43 (20) (20–77)	36 (13) (20–53)	67 (6) (61–77)	25 (9) (20–41)
Male sex	7	3	2	2
BMI kg/m^{-2}	26 (4) (18–30)	27 (3) (21–30)	26 (5) (18–30)	25 (3) (21–29)
FEV_1 $\%_{pred}$	69 (23) (31–108)	91 (16) (72–108)	42 (11) (31–61)	74 (4) (69–79)
FVC $\%_{pred}$	87 (12) (65–110)	96 (13) (77–110)	78 (11) (65–90)	87 (1) (85–89)
FEV_1/FVC	64 (18) (27–86)	77 (8) (65–86)	41 (9) (27–51)	73 (6) (65–80)
TLC $\%_{pred}$	114 (21) (94–175)†	100 (5) (97–108)	129 (27) (106–175)	111 (12) (94–120)*
IC $\%_{pred}$	101 (18) (71–138)†	113 (15) (98–138)	86 (11) (71–96)	104 (18) (90–128)*
FRC $\%_{pred}$	121 (44) (65–243)†	88 (15) (65–107)	164 (45) (132–243)	109 (23) (88–139)*
RV $\%_{pred}$	157 (55) (82–285)†	108 (29) (82–144)	195 (53) (143–285)	172 (42) (109–197)*

$\%_{pred}$, percent predicted; BMI, body mass index; FEV_1, forced expiratory volume in 1 second; FRC, functional residual capacity; FVC, forced vital capacity; IC, inspiratory capacity; SD, standard deviation; TLC, total lung capacity; RV, reserve volume.

*n = 4.

†n = 14.

For this reason, a hierarchical K-means clustering method (32), similar to previously described methods for ^{3}He MRI segmentation (33,34), was used to partition the signal intensity frequency distribution histogram into four clusters, based on an expert chest radiologist's interpretation of the clinical meaning of the visible signal intensity differences. Because the first round of K-means clustering resulted in a single cluster C1 that included both signal void and hypointense regions (partial volumes and/or partially ventilated volumes), K-means clustering was reapplied to the C1 to separate signal void from the hypointense signal regions. This was accomplished in three steps as follows: 1) K-means with four clusters was initially applied to the ^{3}He image, 2) K-means with four clusters was then reapplied to C1, and 3) the first two clusters from step 2 were merged to represent the background and ventilation defects and the last two clusters from step 2 were merged to represent the hypointense signal regions. For both steps 1 and 2, a standard initialization method was performed to produce the initial centroids by dividing the full pixel range of 0–255 into four equal regions: 0–63, 64–127, 128–191, 192–255, and selecting the interval center as the centroid for each cluster.

^{1}H MRI Automated Segmentation: Seeded Region-growing

In conventional ^{1}H MRI anatomical images, low ^{1}H density in the lung produces a weak MRI signal, thus providing sufficient contrast for segmentation methods such as a SRGA (40) to segment the contour of the thoracic cavity to differentiate ventilation defects from the edge of the lung. Before application of SRGA, all ^{1}H images were preprocessed to protect the region-growing algorithm from leaking into regions extending beyond the lung boundary with similar signal intensities. Preprocessing of the ^{1}H images was performed using a two-dimensional radially symmetric Gaussian low-pass filter of size 15×15 with standard deviation 2.0. The images were then converted to a binary mask using a threshold that was selected equal to the half the maximum intensity of the first cluster of K-mean clustering with four clusters. Seed points were then automatically selected in both the left and right lungs of the binary mask by finding the columns in the image binary mask that contained 20 vertically adjacent pixels. A morphological closing algorithm with a structuring element disk of radius equal to 15 (function *imclose* in MATLAB) was applied to fill areas within the segmented left and right lung separately.

Landmark-based Image Registration

Because of the extensive coaching to minimize the potential for differences in the levels of inspiration between the breath-hold scans for all subjects, ^{3}He and ^{1}H images were registered using a landmark-based image affine registration approach (39). Briefly, the center slices, defined as the two-dimensional MRI slice that clearly showed the carina and primary bronchi, were first displayed side-by-side. Three to seven fiducial markers were selected on the ^{3}He image based on the carina, trachea, and primary bronchi as well as any other distinguishing features located within the lung or near the lung periphery such as pulmonary vessels and regions near the diaphragm. The same landmarks were selected in the same order on the ^{1}H image. Geometric operations consisting of rotation, translation, and scaling (same in both x and y directions) were used to transform the ^{1}H image to align it with the corresponding landmarks selected in the ^{3}He image. The same transformation map was applied to the remaining ^{1}H MRI slices. ^{3}He VDV was generated using the lowest signal intensity cluster (C1) and ^{3}He VV was generated as the sum of the remaining clusters (C2–C5).

Statistical Analysis

A two-way analysis of variance was performed for comparison of manual and semiautomated volume measurements with segmentation method and repetition (five repeated measurements) treated as within subject factors using SPSS 16.00

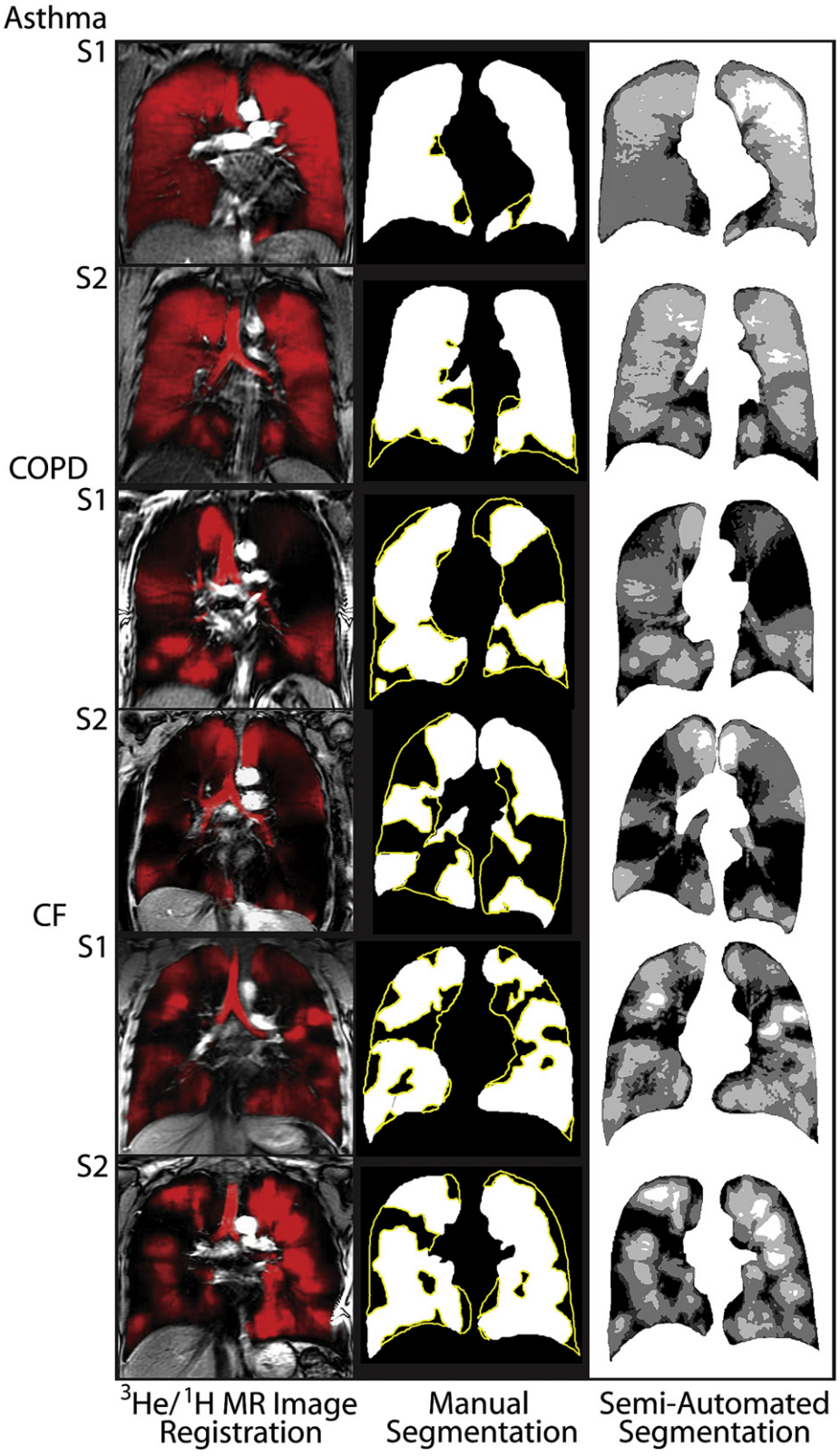

Figure 2. Manual and semiautomated segmentation results for representative asthma, chronic obstructive pulmonary disease (COPD), and cystic fibrosis (CF) subjects. Hyperpolarized helium-3 (^{3}He) magnetic resonance imaging (MRI) center slice registered to ^{1}H MRI, ^{3}He ventilation defect volume, and ventilation volume mask generated by manual segmentation, and ^{3}He cluster map generated by semiautomated segmentation for two representative asthma, COPD, and CF subjects.

(SPSS Inc., Chicago, IL). The relationship between manual and semiautomated segmentation was also determined using linear regression (r^2) and Pearson correlation coefficients (r) and the agreement between the methods was determined using Bland-Altman analysis using GraphPad Prism version 4.00 (GraphPad Software Inc, San Diego, CA). Intraobserver and interobserver reproducibility was determined for manual and semiautomated segmentation results using the coefficient

of variation (CV), calculated as the standard deviation (SD) of the five measurements divided by the mean. Two-way random effects single measure intraclass correlation coefficients (ICC) (absolute agreement) were also determined for the five repeated measurements for both manual and semiautomated segmentation using SPSS 16.00. The 95% confidence intervals (CI) for CV and ICC were determined using the modified McKay's method (41) using SPSS version 16.00. To compare the reproducibility of manual and semiautomated measurements, approximate tests were performed by examining the overlap in 95% CI. The smallest detectable difference (SDD), defined as the smallest difference that can be measured with prospectively determined confidence not due to measurement error (variability), was calculated using the manual and semiautomated five repeated ^{3}He measurements according to Eliasziw et al (42) and shown in equation 1:

$$SDD \geq z_\alpha \sqrt{2} SEM_{intra} \quad (1)$$

where z_α is 1.96 corresponding to a significance level of α = .05 and SEM_{intra} is the standard error of measurement from intraobserver variability and was calculated as shown in equation 2:

$$SEM_{intra} = \sqrt{\hat{\sigma}_e^2} \quad (2)$$

where $\hat{\sigma}_e^2$ is the intraobserver repeated measures variance. The Dice coefficient (43), calculated as the area of the intersection of two datasets divided by the average area of the two sets, was determined to measure the agreement or similarity between each of the five repeated measurements for both manual and semiautomated segmentation (5 repetitions = 10 comparisons) as well as between each of the repeated manual and semiautomated segmentation measurements (5 repetitions for manual and semiautomated = 25 comparisons) as shown in equation 3:

$$Dice(A, B) = \frac{2|A \cap B|}{|A| + |B|} \quad (3)$$

where A and B are the two data sets. For semiautomated segmentation, two observers performed all measurements and therefore the mean Dice coefficient for the two observers was used. In all statistical analyses, results were considered significant when the probability of making a type I error was less than 5% ($P < .05$).

RESULTS

Subject Demographics

Demographic characteristics are provided in Table 1 for 15 subjects in total including five subjects with asthma (n = 3 males, mean age = 36 [±13], range = 20–53), five subjects with COPD (n = 2 males, mean age = 67 [±6], range = 61–77) and five subjects with CF (n = 2 males, mean age = 25 [±9], range = 20–41). COPD subjects were GOLD stage II (n = 1) and GOLD stage III (n = 4).

TABLE 2. Manual and Semiautomated ^{3}He Volume Measurements

Parameter	All (n = 15)	Asthma (n = 5)	COPD (n = 5)	CF (n = 5)
Manual				
VDV L (±SD)	0.92 (0.80)	0.13 (0.15)	1.40 (0.68)	1.23 (0.74)
VV L (±SD)	4.19 (0.53)	4.37 (0.34)	4.12 (0.73)	4.08 (0.52)
Semiautomated				
VDV L* (±SD)	0.76 (0.55)	0.26 (0.19)	1.26 (0.45)	0.76 (0.45)
VV L* (±SD)	4.26 (0.61)	4.43 (0.83)	3.99 (0.90)	4.37 (1.05)
C2 L (±SD)	0.66 (0.17)	0.51 (0.06)	0.80 (0.07)	0.68 (0.20)
C3 L (±SD)	1.77 (0.41)	1.64 (0.43)	1.81 (0.35)	1.86 (0.50)
C4 L (±SD)	1.27 (0.33)	1.55 (0.17)	0.98 (0.32)	1.28 (0.22)
C5 L (±SD)	0.56 (0.20)	0.73 (0.17)	0.41 (0.16)	0.54 (0.13)

C2, cluster 2; C3, cluster 3; C4, cluster 4; C5, cluster 5; SD, standard deviation; VDV, ventilation defect volume; VV, ventilation volume.

*Semiautomated VDV, cluster 1; semiautomated VV, sum of clusters 2–5.

Manual and Semiautomated Measurements

Figure 2 shows the center coronal ^{3}He MRI slice, where the trachea and two main bronchi are clearly visible, for each of two representative asthma, COPD, and CF subjects; ^{3}He ventilation displayed in red registered to the grayscale ^{1}H MRI of the thorax, with the segmentation results obtained by manual and semiautomated segmentation. It is important to note that manual segmentation of the ^{3}He images required approximately 60–90 minutes for all slices per subject, whereas semiautomated ^{3}He segmentation required approximately 4–8 minutes of supervised computational time for all slices per subject.

Table 2 shows the mean whole-lung ^{3}He volume measurements for manual and semiautomated segmentation. There was no significant difference between manual VDV and semiautomated VDV (C1) for asthma, COPD, and CF subjects (P = .10). There was also no significant difference between manual VV and semiautomated VV (C2–C5) for asthma, COPD and CF (P = .48).

Correlations and Bland-Altman Analysis

Figure 3 shows the correlations and Bland-Altman plots between manual and semiautomated VDV. Manual VDV was significantly and highly correlated with semiautomated VDV for asthma (r = 0.89, $P < .0001$), COPD (r = 0.84, $P < .0001$), and CF subjects (r = 0.89, $P < .0001$). Bland-Altman analysis indicated that there was negligible bias between manual and semiautomated VDV for asthma (bias = −0.01 ± 0.01L), COPD (bias = 0.01 ± 0.05L), and CF subjects (0.05 ± 0.04L).

Figure 4 shows the correlations and Bland-Altman plots between manual and semiautomated VV. Manual VV was significantly and highly correlated with semiautomated VV

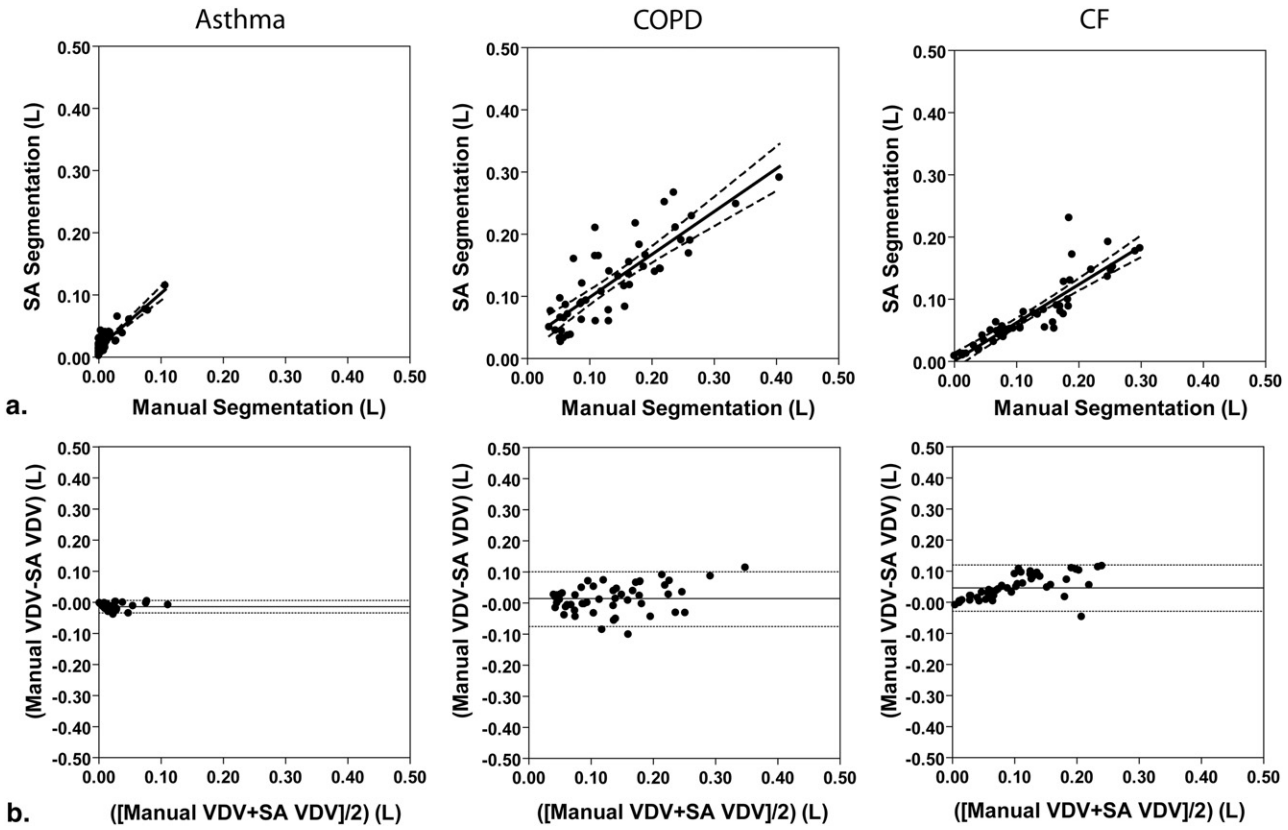

Figure 3. Correlations and Bland-Altman plots between manual and semiautomated ventilation defect volume (VDV) for all slices. **(a)** Manual VDV was significantly correlated with semiautomated VDV for asthma ($r = 0.89$, $P < .0001$, $r^2 = 0.80$, $P < .0001$, y = 0.87x + 0.02), COPD ($r = 0.84$, $P < .0001$, $r^2 = .70$, $P < .0001$, y = 0.69x + 0.03), and CF subjects ($r = 0.89$, $P < .0001$, $r^2 = 0.79$, $P < .0001$, y = 0.61x + 0.001). **(b)** The mean difference (±SD) between manual and semiautomated VDV was −0.01L ± 0.01L (lower limit = −0.03L, upper limit = −0.0006L), 0.01L ± 0.05L (lower limit = −0.08L, upper limit = −0.10L), and 0.05L ± 0.04L (lower limit = −0.03L, upper limit = −0.12L) for asthma, COPD, and CF subjects, respectively. *Solid lines* indicate the mean difference and *dotted lines* indicate the 95% limits of agreement.

for asthma ($r = 0.99$, $P < .0001$), COPD ($r = 0.91$, $P < .0001$), and CF subjects ($r = 0.84$, $P < .0001$). Bland-Altman analysis indicated that there was negligible bias for manual and semiautomated VV for asthma (bias = −0.003 ± 0.02 L), COPD (bias = 0.01 ± 0.04 L), and CF subjects (−0.03 ± 0.06 L).

Reproducibility

Table 3 shows the intraobserver reproducibility of ^{3}He volume measurements for manual and semiautomated segmentation for all subjects. Intraobserver reproducibility was significantly higher for semiautomated VDV compared to manual VDV as indicated by the nonoverlapping 95% CI for both CV (manual: CV = 12%, 95% CI = 9%–19%, semiautomated: CV = 5%, 95% CI = 4%–8%) and ICC (manual: ICC = 0.98, 95% CI = 0.96–0.99, semiautomated: ICC = 1.00, 95% CI = 0.99–1.00). Intraobserver reproducibility was also significantly higher for semiautomated VV compared to manual VV as indicated by the nonoverlapping 95% CI for both CV (manual: CV = 4%, 95% CI = 3%–7%, semiautomated: CV = 0.2%, 95% CI = 0.2%–0.4%), and ICC (manual: ICC = 0.90, 95% CI = 0.81–0.96, semiautomated: ICC = 1.00, 95% CI = 1.00–1.00).

Table 4 shows the interobserver reproducibility of ^{3}He volume measurements for semiautomated segmentation for all subjects. For the two observers, CV was low (VDV: CV = 7%, 95% CI = 5%–11%, VV: CV = 0.4%, 95% CI = 0.3%–0.6%) and ICC was high (VDV: ICC = 0.96, 95% CI = 0.76–0.99, VV: ICC = 1.00, 95% CI = 0.83–1.00) across all three respiratory diseases evaluated.

Smallest Detectable Difference

Table 5 shows the SDD for measurements obtained by manual and semiautomated segmentation. For manual segmentation, the SDD or the minimum change that could be measured confidently in individual asthma, COPD, and CF subjects that were not due to technological or observer measurement variability (measurement error) was 310 mL and 480 mL for ^{3}He VDV and VV, respectively. For the semiautomated method, the SDD or the minimum change that could be measured confidently in individual asthma, COPD and CF subjects was 110 mL and 30 mL for ^{3}He VDV and VV, respectively.

Dice Coefficients

Table 6 shows the Dice coefficients for manual and semiautomated segmentation. Dice coefficients (D) were higher for

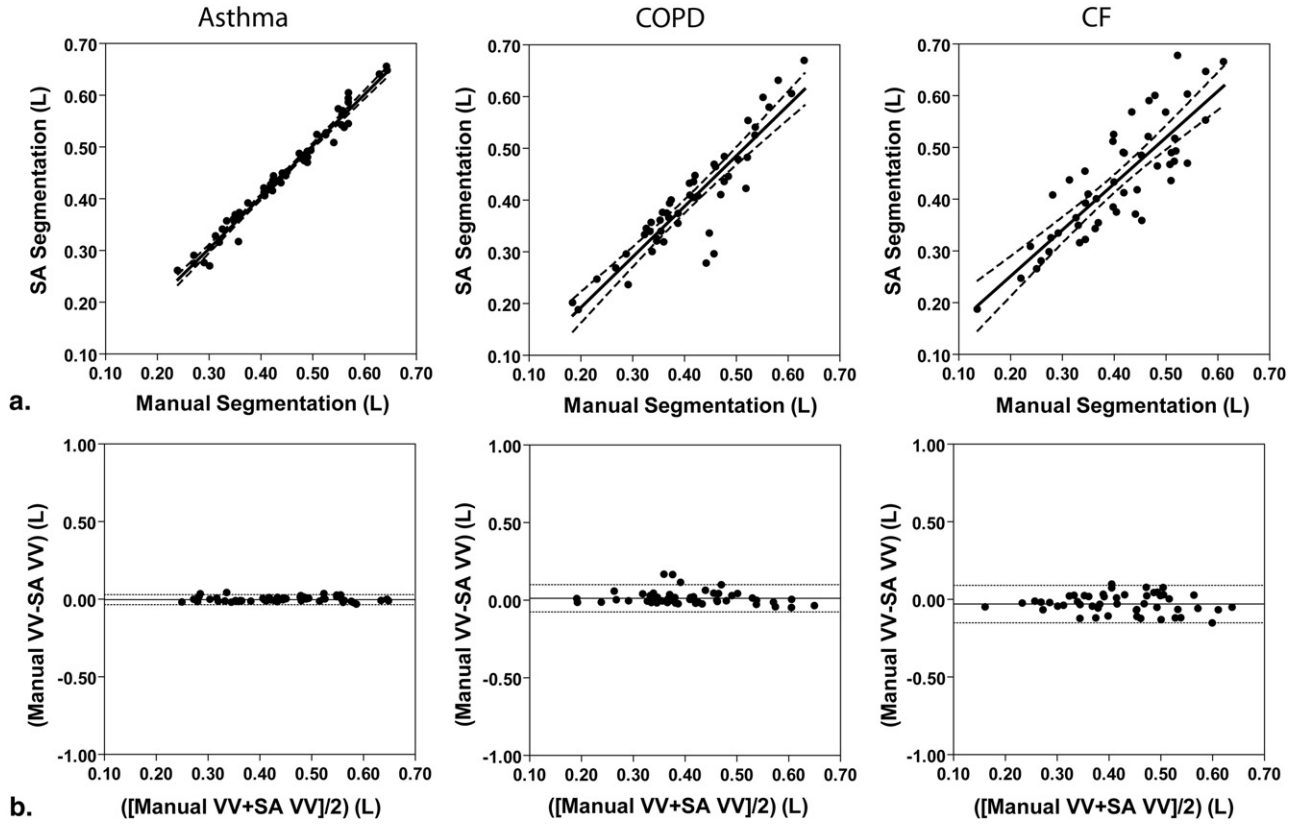

Figure 4. Correlations and Bland-Altman plots between manual and semiautomated ventilation volume (VV) for all slices. **(a)** Manual VV was significantly correlated with semiautomated VV for asthma ($r = 0.99$, $P < .0001$, $r^2 = 0.98$, $P < .0001$, $y = 0.99x + 0.005$), chronic obstructive pulmonary disease (COPD) ($r = 0.91$, $P < .0001$, $r^2 = 0.83$, $P < .0001$, $y = 0.98x - 0.003$), and cystic fibrosis (CF) subjects ($r = 0.84$, $P < .0001$, $r^2 = 0.71$, $P < .0001$, $y = 0.89x + 0.07$). **(b)** The mean difference (±SD) between manual and semiautomated VV was -0.003L ± 0.02L (lower limit = -0.03L, upper limit = 0.03L), 0.01L ± 0.04L (lower limit = -0.08L, upper limit = -0.10L), and -0.03L ± 0.06L (lower limit = -0.15L, upper limit = 0.09L) for asthma, COPD, and CF subjects, respectively. *Solid lines* indicate the mean difference and *dotted lines* indicate the 95% limits of agreement.

repeated semiautomated segmentation than for repeated manual segmentation measurements for both VDV (manual: D = 0.71; semiautomated: D = 0.88) and VV (manual: D = 0.95; semiautomated: D = 1.00). The Dice coefficient for manual and semiautomated VDV was 0.44 and the Dice coefficient for manual and semiautomated VV was 0.91.

DISCUSSION

In contrast to the homogenous ^{3}He MRI signal intensity observed in healthy subjects with normal lung function, ^{3}He MRI of subjects with respiratory disease results in heterogeneous signal intensity throughout the lung, which may be a result of small airway occlusion, mucous plugs, airway wall thickening, and inflammation or bullous disease. Related to this is that there is significant functional information in the regions of middle-intensity, and both hyper- and hypointense signal regions that have not yet been quantitatively or spatially exploited. The development and validation of ^{3}He image analysis techniques, or the use of widely available and well-established image processing algorithms, that quantify heterogeneous signal information are required to fully characterize the important ventilation information contained in the image, and may enable a better understanding of the physiological changes that occur in disease longitudinally and in response to treatment. Here we evaluated the spatial and quantitative agreement of a semiautomated segmentation method with manual segmentation for the evaluation of ^{3}He and ^{1}H MRI of asthma, COPD, and CF subjects and report: 1) ^{3}He manual and semiautomated VDV and VV measurements that were not statistically significantly different, and were significantly correlated with good agreement; 2) significantly higher intraobserver reproducibility for semiautomated compared to manual measurements and high interobserver reproducibility; 3) smallest detectable differences that were lower for semiautomated measurements; and 4) high Dice coefficients for manual and semiautomated VV, indicating excellent spatial overlap.

^{3}He MRI measurements for asthma, COPD, and CF subjects generated by manual and semiautomated segmentation were not significantly different and were significantly and strongly correlated and in good agreement. A small but insignificant bias was detected by Bland-Altman analysis that may be due to the manual observers' tendency to classify

TABLE 3. Intraobserver Reproducibility of Manual and Semiautomated ^{3}He Volume Measurements

Parameter	All (n = 15)	Asthma (n = 5)	COPD (n = 5)	CF (n = 5)
Manual				
VDV				
CV % (95% CI)	12 (9–19)	9 (5–26)	9 (5–25)	12 (7–36)
ICC (95% CI)	0.98 (0.96–0.99)	0.99 (0.98–1.00)	0.97 (0.90–1.00)	0.96 (0.87–1.00)
VV				
CV % (95% CI)	4 (3–7)	2 (1–5)	5 (3–13)	6 (3–16)
ICC (95% CI)	0.90 (0.81–0.96)	0.96 (0.85–1.00)	0.94 (0.68–0.99)	0.83 (0.56–0.98)
Semiautomated				
VDV*				
CV % (95% CI)	5 (4–8)	6 (4–18)	4 (3–13)	4 (2–11)
ICC (95% CI)	1.00 (0.99–1.00)	0.99 (0.97–1.00)	0.98 (0.95–1.00)	1.00 (0.98–1.00)
VV*				
CV % (95% CI)	0.2 (0.2–0.4)	0.2 (0.1–0.5)	0.2 (0.0–0.1)	0.4 (0.2–1.1)
ICC (95% CI)	1.00 (1.00–1.00)	1.00 (1.00–1.00)	1.00 (1.00–1.00)	1.00 (1.00–1.00)
C2				
CV % (95% CI)	0.6 (0.5–1)	1 (0.5–2)	0.3 (0.2–1)	1 (0.5–2)
ICC (95% CI)	1.00 (1.00–1.00)	0.99 (0.97–1.00)	1.00 (1.00–1.00)	1.00 (1.00–1.00)
C3				
CV % (95% CI)	0.3 (0.2–0.5)	0.2 (0.1–0.6)	0.2 (0.1–0.3)	0.5 (0.3–1)
ICC (95% CI)	1.00 (1.00–1.00)	1.00 (1.00–1.00)	1.00 (0.99–1.00)	1.00 (0.99–1.00)
C4				
CV % (95% CI)	0.1 (0.1–0.2)	0.1 (0.0–0.2)	0.1 (0.1–0.4)	0.2 (0.1–0.6)
ICC (95% CI)	1.00 (1.00–1.00)	1.00 (0.99–1.00)	1.00 (1.00–1.00)	1.00 (0.99–1.00)
C5				
CV % (95% CI)	0.1 (0.0–0.1)	0.1 (0.0–0.2)	0.0 (0.0–0.1)	0.1 (0.1–0.2)
ICC (95% CI)	1.00 (1.00–1.00)	1.00 (1.00–1.00)	1.00 (1.00–1.00)	1.00 (1.00–1.00)

C2, cluster 2; C3, cluster 3; C4, cluster 4; C5, cluster 5; CI, confidence interval; CV, coefficient of variation; ICC, intraclass correlation coefficient; VDV, ventilation defect volume; VV, ventilation volume.

*Semiautomated VDV, cluster 1; semiautomated VV, sum of clusters 2–5.

hypoventilated areas as defects in some subjects and in some image slices and not in others, or the inclusion of regions of signal loss associated with the pulmonary vascular structures, not included with manual segmentation (38), by the K-means approach. However, it is important to note that the inclusion of pulmonary vascular structures because ventilation defects may not be a critical consideration for serial studies. The improvement in segmentation time afforded by the semiautomated approach and the finding that the lung can be reliably segmented in a number of respiratory diseases, demonstrates the potential for ^{3}He MRI segmentation in large-scale, multicenter clinical evaluations.

We also observed that intraobserver reproducibility of the ^{3}He measurements was significantly higher for semiautomated segmentation compared to the manual approach, and interobserver reproducibility was high for the semiautomated method and higher than previously reported manual results (44). Clearly, segmentation methods that provide high intra- and interobserver reproducibility are required for future studies involving large subject numbers and multiple research centers such that reliable measurements can be obtained from multiple observers independent of the level of experience. To better understand if the improvements in measurement reproducibility afforded by semiautomated segmentation could be translated to practical use, the SDD was determined for both manual and semiautomated measurements, and the semiautomated method developed here reported a lower SDD as compared to manual results. For serial studies, it is important to be confident that the changes measured between imaging time points are not due to measurement error. Therefore, future ^{3}He serial studies should use segmentation methods with low measurement error to detect the important functional measurement changes that occur after intervention or during disease progression. Furthermore, the excellent reproducibility and very low SDD for ^{3}He VV suggests that this measurement could be used in future studies for the analysis of treatment effects in individual subjects.

Finally, we demonstrated high Dice coefficients between the semiautomated and manual segmentation results. This finding suggests that along with the higher intra- and interobserver reproducibility of the volume measurements obtained by the semiautomated method, the segmentation results are also highly spatially reproducible. However, we also reported low Dice coefficients between the manual and semiautomated VDV segmentation results for the asthma subjects and moderate Dice coefficients for the COPD and CF subjects. The lack of spatial correspondence between the two methods, particularly in the asthma subjects, is likely from the small size

TABLE 4. Interobserver Reproducibility of Semiautomated ^{3}He Volume Measurements

Parameter	All (*n* = 15)	Asthma (*n* = 5)	COPD (*n* = 5)	CF (*n* = 5)
VDV*				
CV % (95% CI)	7 (5–11)	12 (7–37)	6 (4–17)	5 (3–15)
ICC (95% CI)	0.96 (0.76–0.99)	0.95 (0.02–1.00)	0.94 (0.43–0.99)	0.97 (0.41–1.00)
VV*				
CV % (95% CI)	0.4 (0.3–0.6)	0.2 (0.1–0.6)	0.2 (0.1–0.7)	0.5 (0.3–1.5)
ICC (95% CI)	1.00 (0.83–1.00)	0.99 (0.60–1.00)	1.00 (0.79–1.00)	1.00 (0.85–1.00)
C2				
CV % (95% CI)	1 (0.6–1)	1 (1–3)	0.5 (0.3–1)	1 (1–3)
ICC (95% CI)	0.99 (0.54–1.00)	0.92 (0.03–0.99)	0.98 (0.08–1.00)	0.99 (0.25–1.00)
C3				
CV % (95% CI)	0.5 (0.3–0.7)	0.3 (0.2–0.9)	0.3 (0.2–0.8)	0.6 (0.4–1.9)
ICC (95% CI)	1.00 (0.92–1.00)	1.00 (0.96–1.00)	1.00 (0.78–1.00)	1.00 (0.98–1.00)
C4				
CV % (95% CI)	0.2 (0.2–0.3)	0.1 (0.1–0.2)	0.2 (0.1–0.6)	0.3 (0.9–0.2)
ICC (95% CI)	1.00 (1.00–1.00)	1.00 (1.00–1.00)	1.00 (1.00–1.00)	1.00 (1.00–1.00)
C5				
CV % (95% CI)	0.1 (0.1–0.2)	0.1 (0.1–0.2)	0.0 (0.0–0.1)	0.1 (0.1–0.4)
ICC (95% CI)	1.00 (1.00–1.00)	1.00 (1.00–1.00)	1.00 (1.00–1.00)	1.00 (1.00–1.00)

C2, cluster 2; C3, cluster 3; C4, cluster 4; C5, cluster 5; CI, confidence interval; CV, coefficient of variation; ICC, intraclass correlation coefficient; VDV, ventilation defect volume; VV, ventilation volume.

*Semiautomated VDV, cluster 1; semiautomated VV, sum of clusters 2–5.

TABLE 5. Smallest Detectable Difference for Manual and Semiautomated Segmentation

Parameter	All (*n* = 15)	Asthma (*n* = 5)	COPD (*n* = 5)	CF (*n* = 5)
Manual				
VDV L (±SD)	0.31	0.03	0.34	0.42
VV L (±SD)	0.48	0.20	0.52	0.63
Semiautomated				
VDV* L (±SD)	0.11	0.05	0.16	0.08
VV* L (±SD)	0.03	0.02	0.02	0.05
C2 L (±SD)	0.01	0.01	0.01	0.02
C3 L (±SD)	0.02	0.01	0.01	0.02
C4 L (±SD)	0.01	0.00	0.00	0.01
C5 L (±SD)	0.00	0.00	0.00	0.00

C2, cluster 2; C3, cluster 3; C4, cluster 4; C5, cluster 5; VDV, ventilation defect volume; VV, ventilation volume.

*Semiautomated VDV, cluster 1; semiautomated VV, sum of clusters 2–5.

TABLE 6. Dice Coefficients for Manual and Semiautomated Segmentation

Parameter	All (*n* = 15)	Asthma (*n* = 5)	COPD (*n* = 5)	CF (*n* = 5)
Manual–manual				
VDV	0.71 (0.09)†	0.69 (0.12)	–	0.74 (0.05)
VV	0.95 (0.03)†	0.97 (0.00)	–	0.92 (0.02)
Semiautomated–semiautomated				
VDV*	0.88 (0.06)	0.82 (0.03)	0.92 (0.04)	0.89 (0.06)
VV*	1.00 (0.00)	1.00 (0.00)	1.00 (0.00)	1.00 (0.00)
Manual–semiautomated				
VDV	0.44 (0.28)	0.15 (0.15)	0.52 (0.10)†	0.65 (0.25)
VV	0.91 (0.05)	0.95 (0.01)	0.88 (0.08)	0.90 (0.03)

C2, cluster 2; C3, cluster 3; C4, cluster 4; C5, cluster 5; CI, confidence interval; CV, coefficient of variation; ICC, intraclass correlation coefficient; VDV, ventilation defect volume; VV, ventilation volume.

*Semiautomated VDV, cluster 1; semiautomated VV, sum of clusters 2–5.

†One repetition of manual segmentation.

of the ventilation defects. It should be noted that K-means clustering is a histogram-based segmentation approach, thus very small areas of signal void may be included as defects by the semiautomated method but overlooked because of the small size by the manual observer. Therefore, the excellent spatial and quantitative agreement between manual and semiautomated segmentation suggests that semiautomated or automated segmentation methods are important for future ^{3}He imaging studies and should be used as we transition to ^{129}Xe MRI.

Although the semiautomated ^{3}He segmentation method is very promising, we must acknowledge that the physiological rationale for selecting the initial cluster number was based on the expert observer's visual assessment, not on a more objective approach. However, we have previously evaluated K-means with the initial user input of 4–10 clusters and the hierarchical K-means approach described here and determined that hierarchical K-means provided the highest correlation and lowest Bland-Altman bias with manual segmentation.

In conclusion, we employed a straightforward combination of previously developed, well-described, and widely available methods, namely hierarchical K-means, seeded region-

growing, and nonrigid registration, to ^{3}He MRI to enable semiautomated segmentation of the unique functional information this method provides. Reproducible and robust segmentation methods that can be applied across many respiratory conditions are urgently needed for larger scale pulmonary functional MRI studies.

REFERENCES

1. Parraga G, Ouriadov A, Evans A, et al. Hyperpolarized 3He ventilation defects and apparent diffusion coefficients in chronic obstructive pulmonary disease: preliminary results at 3.0 Tesla. Invest Radiol 2007; 42:384–391.
2. de Lange EE, Mugler JP III, Brookeman JR, et al. Lung air spaces: MR imaging evaluation with hyperpolarized 3He gas. Radiology 1999; 210: 851–857.
3. Kauczor HU, Ebert M, Kreitner KF, et al. Imaging of the lungs using 3He MRI: preliminary clinical experience in 18 patients with and without lung disease. J Magn Reson Imaging 1997; 7:538–543.
4. Moller HE, Chen XJ, Saam B, et al. MRI of the lungs using hyperpolarized noble gases. Magn Reson Med 2002; 47:1029–1051.
5. Kirby M, Mathew L, Wheatley A, et al. Chronic obstructive pulmonary disease: longitudinal hyperpolarized (3)He MR imaging. Radiology 2010; 256:280–289.
6. Choy S, Wheatley A, McCormack DG, et al. Hyperpolarized 3He magnetic resonance imaging derived pulmonary pressure-volume curves. J Appl Physiol 2010; 109:574–585.
7. Mathew L, Kirby M, Etemad-Rezai R, et al. Hyperpolarized (3)He magnetic resonance imaging: preliminary evaluation of phenotyping potential in chronic obstructive pulmonary disease. Eur J Radiol 2011; 79:140–146.
8. Mathew L, Evans A, Ouriadov A, et al. Hyperpolarized 3He magnetic resonance imaging of chronic obstructive pulmonary disease: reproducibility at 3.0 tesla. Acad Radiol 2008; 15:1298–1311.
9. Evans A, McCormack DG, Santyr G, et al. Mapping and quantifying hyperpolarized 3He magnetic resonance imaging apparent diffusion coefficient gradients. J Appl Physiol 2008; 105:693–699.
10. de Lange EE, Altes TA, Patrie JT, et al. Evaluation of asthma with hyperpolarized helium-3 MRI: correlation with clinical severity and spirometry. Chest 2006; 130:1055–1062.
11. Altes TA, Powers PL, Knight-Scott J, et al. Hyperpolarized 3He MR lung ventilation imaging in asthmatics: preliminary findings. J Magn Reson Imaging 2001; 13:378–384.
12. Fain SB, Gonzalez-Fernandez G, Peterson ET, et al. Evaluation of structure-function relationships in asthma using multidetector CT and hyperpolarized He-3 MRI. Acad Radiol 2008; 15:753–762.
13. Tzeng YS, Lutchen K, Albert M. The difference in ventilation heterogeneity between asthmatic and healthy subjects quantified using hyperpolarized 3He MRI. J Appl Physiol 2009; 106:813–822.
14. Mentore K, Froh DK, de Lange EE, et al. Hyperpolarized HHe 3 MRI of the lung in cystic fibrosis: assessment at baseline and after bronchodilator and airway clearance treatment. Acad Radiol 2005; 12:1423–1429.
15. Koumellis P, Van Beek EJ, Woodhouse N, et al. Quantitative analysis of regional airways obstruction using dynamic hyperpolarized 3He MRI-preliminary results in children with cystic fibrosis. J Magn Reson Imaging 2005; 22:420–426.
16. Donnelly LF, MacFall JR, McAdams HP, et al. Cystic fibrosis: combined hyperpolarized 3He-enhanced and conventional proton MR imaging in the lung–preliminary observations. Radiology 1999; 212:885–889.
17. Mathew L, Gaede S, Wheatley A, et al. Detection of longitudinal lung structural and functional changes after diagnosis of radiation-induced lung injury using hyperpolarized 3He magnetic resonance imaging. Med Phys 2010; 37:22–31.
18. Ireland RH, Bragg CM, McJury M, et al. Feasibility of image registration and intensity-modulated radiotherapy planning with hyperpolarized helium-3 magnetic resonance imaging for non-small-cell lung cancer. Int J Radiat Oncol Biol Phys 2007; 68:273–281.
19. Zaporozhan J, Ley S, Gast KK, et al. Functional analysis in single-lung transplant recipients: a comparative study of high-resolution CT, 3He-MRI, and pulmonary function tests. Chest 2004; 125:173–181.
20. McAdams HP, Palmer SM, Donnelly LF, et al. Hyperpolarized 3He-enhanced MR imaging of lung transplant recipients: preliminary results. AJR Am J Roentgenol 1999; 173:955–959.
21. Wild JM, Schmiedeskamp J, Paley MNJ, et al. MR imaging of the lungs with hyperpolarized helium-3 gas transported by air. Phys Med Biol 2002; 47:N185–N190.
22. Teh K, Lee KJ, Paley MNJ, et al. Parallel imaging of hyperpolarized helium-3 with simultaneous slice excitation. Magn Reson Med 2006; 55:258–262.
23. Wild JM, Woodhouse N, Teh K. Single-scan acquisition of registered hyperpolarized He-3 ventilation and ADC images using a hybrid 2D gradient-echo sequence. Magn Reson Med 2007; 57:1185–1189.
24. Wild JM, Ajraoui S, Deppe MH, et al. Synchronous acquisition of hyperpolarised (3) He and (1) H MR images of the lungs—maximising mutual anatomical and functional information 1. NMR Biomed 2011; 24:130–134.
25. Salerno M, Altes TA, Brookeman JR, et al. Dynamic spiral MRI of pulmonary gas flow using hyperpolarized (3)He: preliminary studies in healthy and diseased lungs. Magn Reson Med 2001; 46:667–677.
26. Saam B, Yablonskiy DA, Gierada DS, et al. Rapid imaging of hyperpolarized gas using EPI. Magn Reson Med 1999; 42:507–514.
27. Woodhouse N, Wild JM, Paley MN, et al. Combined helium-3/proton magnetic resonance imaging measurement of ventilated lung volumes in smokers compared to never-smokers. J Magn Reson Imaging 2005; 21: 365–369.
28. Tustison NJ, Altes TA, Song G, et al. Feature analysis of hyperpolarized helium-3 pulmonary MRI: a study of asthmatics versus nonasthmatics. Magn Reson Med 2010; 63:1448–1455.
29. Ray N, Acton ST, Altes T, et al. Merging parametric active contours within homogeneous image regions for MRI-based lung segmentation. IEEE Trans Med Imaging 2003; 22:189–199.
30. Kauczor HU, Markstaller K, Puderbach M, et al. Volumetry of ventilated airspaces by 3He MRI: preliminary results. Invest Radiol 2001; 36:110–114.
31. Adams R, Bischof L. Seeded region growing. IEEE Trans Pattern Anal Machine Intell 1994; 16:641–647.
32. MacQueen J. Some Methods for Classification and Analysis of Multivariate Observations. Proceedings of 5th Berkeley Symposium on Mathematical Statistics and Probability, University of California Press; 1967. p. 281–297.
33. Cooley B, Acton S, Salerno M, et al. Automated scoring of hyperpolarized helium-3 MR lung ventilation images: initial development and validation. Proc Intl Soc Mag Reson Med Honolulu, Hawaii, May 18-25, 2002.
34. Guyer RA, Hellman MD, Emami K, et al. A robust method for estimating regional pulmonary parameters in presence of noise. Acad Radiol 2008; 15:740–752.
35. Rabe KF, Hurd S, Anzueto A, et al. Global strategy for the diagnosis, management, and prevention of chronic obstructive pulmonary disease: GOLD executive summary. Am J Respir Crit Care Med 2007; 176:532–555.
36. Walter SD, Eliasziw M, Donner A. Sample size and optimal designs for reliability studies. Stat Med 1998; 17:101–110.
37. Landry A, Spence JD, Fenster A. Quantification of carotid plaque volume measurements using 3D ultrasound imaging. Ultrasound Med Biol 2005; 31:751–762.
38. de Lange EE, Altes TA, Patrie JT, et al. The variability of regional airflow obstruction within the lungs of patients with asthma: assessment with hyperpolarized helium-3 magnetic resonance imaging. J Allergy Clin Immunol 2007; 119:1072–1078.
39. Kirby M, Wheatley A, McCormack DG, et al. Development and application of methods to quantify spatial and temporal hyperpolarized 3He MRI ventilation dynamics: preliminary results in chronic obstructive pulmonary disease. Proc SPIE 2010; 7626:762605.
40. Adams LB. Seeded region growing. IEEE Trans Pattern Anal Machine Intell 1994; 16:641–647.
41. Vangel MG. Confidence intervals for a normal coefficient of variation. Am Statistician 1996; 50:21–26.
42. Eliasziw M, Young SL, Woodbury MG, et al. Statistical methodology for the concurrent assessment of interrater and intrarater reliability: using goniometric measurements as an example. Phys Ther 1994; 74:777–788.
43. Dice LR. Measures of the amount of ecologic association between species. Ecology 1945; 26:297–302.
44. Parraga G, Mathew L, Etemad-Rezai R, et al. Hyperpolarized 3He magnetic resonance imaging of ventilation defects in healthy elderly volunteers: initial findings at 3.0 Tesla. Acad Radiol 2008; 15:776–785.

APPENDIX

TABLE. Comparison of ^{3}He VDV and VV Generated by Manual Segmentation with K-Means Clustering with 4 to 10 Clusters and Hierarchical K-Means Using Pearson Correlation Coefficients and Bland-Altman Analysis

	Pearson Correlation Coefficients		Bland-Altman Analysis		
Parameter	*r*	*P* Value	Bias	Lower CI	Upper CI
VDV L					
4 clusters	0.67	.0001	−0.08	−0.06	0.21
5 clusters	0.79	.0001	−0.04	−0.06	0.14
6 clusters	0.73	.0001	−0.02	−0.09	0.14
7 clusters	0.75	.0001	−0.01	−0.10	0.12
8 clusters	0.80	.0001	−0.004	−0.10	0.09
9 clusters	0.76	.0001	−0.01	−0.12	0.10
10 clusters	0.76	.0001	−0.02	−0.12	0.09
Hierarchical K-means	0.84	.0001	−0.006	−0.10	0.08
VV L					
4 clusters	0.80	.0001	−0.09	−0.22	0.03
5 clusters	0.89	.0001	−0.06	−0.15	0.04
6 clusters	0.88	.0001	−0.04	−0.14	0.06
7 clusters	0.89	.0001	−0.03	−0.12	0.07
8 clusters	0.91	.0001	−0.01	−0.11	0.08
9 clusters	0.88	.0001	−0.007	−0.11	0.09
10 clusters	0.88	.0001	−0.001	−0.10	0.10
Hierarchical K-means	0.91	.0001	−0.01	−0.10	0.08

CI, 95% confidence interval; *r*, Pearson correlation coefficient; VDV, ventilation defect volume; VV, ventilation volume.
Significance ($P < .05$).